Diagnosis alfalfa salt stress based on UAV multispectral image texture and vegetation index

Hong Ma
mahong@lut.edu.cn

Lanzhou University of Technology
Wenju Zhao
Haiying Yu
Pengtao Yang
Faqi Yang
Zongli Li

Research Article

Keywords: UAV multispectral, Vegetation index, Texture feature, Soil background, Salt stress diagnosis

Posted Date: December 10th, 2024

DOI: https://doi.org/10.21203/rs.3.rs-4954870/v1

Version of Record: A version of this preprint was published at Plant and Soil on February 18th, 2025. See the published version at https://doi.org/10.1007/s11104-025-07203-1.

Diagnosis alfalfa salt stress based on UAV multispectral image texture and vegetation index

Hong Ma[a,b,c], Wenju Zhao[1a,c*], Haiying Yu[a,c], Pengtao Yang[a,c], Faqi Yang[a,c], Zongli Li[d]

[a.] School of Energy and Power Engineering, Lanzhou University of Technology, Lanzhou 730050, China;
[b.] JiuQuan Vocational Technical College, JiuQuan 735000, China.
[c.] Key Laboratory of Smart Agriculture Irrigation Equipment, Ministry of Agriculture and Rural Affairs, Lanzhou 730050, China;
[d.] General Institute for Water Resources and Hydropower Planning and Design, Ministry of Water Resources, Beijing 100053, China.

* Corresponding author at: College of Energy and Power Engineering, Lanzhou University of Technology, Lanzhou, 730050, China.
Email address: wenjuzhao@lut.edu.cn

Abstract

Aims This study aimed to explore the effects of increasing image texture features and removing soil background on the alfalfa salt stress diagnosis accuracy.

Methods This study extracted spectral reflectance to construct 15 vegetation indexes, and used gray level co-occurrence matrix to calculate eight image texture features. The Canny edge detection algorithm was used to remove the soil background, and set T1 (vegetation index non-removed soil background), T2 (vegetation index+image texture features non-removed soil background), T3 (vegetation index removed soil background), T4 (vegetation index+image texture features removed soil background), as independent variables to construct salt stress diagnosis model based on the support vector regression algorithm, and determined the best salt stress diagnosis model.

Results Compared with the T1, the modeling and validation accuracies of salt stress diagnosis model constructed based on the T2 increased by 13.39% and 13.36%, respectively, and those of salt stress diagnosis model constructed based on the T3 increased by 6.30% and 5.33%. The salt stress diagnosis accuracy constructed based on T4 was the highest, with the modeling set R^2, RMSE, and RPD of 0.675, 0.2143, and 1.7735, respectively, and the validation set R^2, RMSE, and RPD of 0.652, 0.2349, and 15749, respectively. The modeling and validation accuracies of the salt stress diagnosis model constructed based on crop salt stress index (CSSI) reached more than 0.564 and 0.549, respectively, which can be used as a new indicator for diagnosing salt stress.

Conclusions Both increasing image texture features and removing soil background can significantly improve the accuracy of alfalfa salt stress diagnosis.

Key words UAV multispectral; Vegetation index; Texture feature; Soil background; Salt stress diagnosis

1. Introduction

Soil salinization seriously affects crop root respiration and soil structure, resulting in large-scale farmland degradation and crop yield reduction (Steinhorst and Kudla, 2019; Chen et al., 2022). Salt stress not only causes physiological drought of crops, but also inhibits the water conduction of soil-crop system, which seriously hinders the normal crop growth. It is highly important to quickly, accurately and extensively diagnose the salt stress of crops for effective monitoring of their health status and developing high water efficiency agriculture (Gupta et al., 2021; Zhao et al., 2022; Feng et al., 2023). Traditional crop salt stress diagnosis is mainly based on positioning monitoring, which is a complex process. Therefore, it is difficult to diagnose the salt stress status of crops in a large area (Tian et al., 2021; Behera et al., 2022; Shen et al., 2023; Yue et al., 2023). Low-altitude remote sensing provides a scientific and effective technical means for crop growth monitoring. An unmanned aerial vehicle (UAV) is a type of low-altitude remote sensing platform equipped with spectral instruments and has unique advantages such as flexibility, high efficiency and repeatability. It can quickly obtain large-scale image information and realize rapid and large-scale monitoring of crop growth (Sunita et al., 2018; Maes et al., 2019; Maimaitijiang et al., 2020; Qi et al., 2021).

The vegetation index has high correlation with growth parameters such as leaf area index, biomass, chlorophyll content, stomatal conductance and other growth parameters of crops (Mandal et al., 2020; Zhang et al., 2021; Zhang et al., 2023; Li et al., 2023). It can reflect the growth condition of crops that can provide a basis for monitoring their growth process; however, the monitoring accuracy of the growth condition of crops based on the vegetation index is low (Ryu et al., 2020; Ma et al., 2021; Zhang et al., 2021). The UAV multispectral images contain spectral as well as rich image texture information. As an extremely important attribute of remote sensing images, image texture features can effectively reflect the changes in the physical properties of the crop surface. Increasing image texture features can effectively improve the accuracy of crop growth monitoring (Kawamura et al., 2021; Liu et al., 2022; Sun et al., 2023). Freitas et al. (2022) constructed an estimation model of grassland aboveground biomass based on the spectral and texture information of UAV images, and pointed out that image texture information played an important role in aboveground biomass estimation. Ilniyaz et al. (2023) evaluated the potential of UAV imagery in estimating leaf area index in vineyards, and pointed out that texture features performed better than vegetation indices, and the combination of vegetation indices and texture features could improve the estimation results. Yue et al. (2019) evaluated the accuracy of ultra-high resolution UAV image texture and vegetation index, and their combination in the estimation of aboveground biomass of winter wheat. The authors concluded that the combination could improve the accuracy of biomass estimation by 22.63% compared to that without the addition of image texture. Zhou et al. (2021) studied water stress diagnosis in winter wheat based on UAV multispectral vegetation index and image texture, which proved to be a feasible and accurate method. Yuan et al. (2023) explored the effect of spectral and textural information fusion on the accuracy of the model for estimating the leaf area index of rice. The authors extracted the reflectance of the rice canopy and eight textural features calculated using the gray scale covariance matrix. Zhao et al. (2023) explored the effect of combining image texture information and spectral indices on the accuracy of soil salinity inversion model, and pointed out that this combination could effectively improve the inversion accuracy. The aforementioned studies achieved good research results in crop yield estimation, aboveground biomass estimation, leaf area index estimation and water stress diagnosis based on the vegetation index and image texture features. The combination of vegetation index and image texture features for salt stress diagnosis in crops is a useful area for further investigation.

Remote sensing images acquired using UAV remote sensing technology are prone to the problem of soil background interference. It has been shown that removing soil background from these images is an effective way to improve the crop growth monitoring accuracy, which has been widely used in crop nitrogen nutrition and water stress diagnosis (Pan et al., 2023; Wang et al., 2021). Almeida-Ñauñay et al. (2023) explored the effect of soil background on wheat yield estimation accuracy based on the optimization of vegetation index, where the soil background was removed using threshold optimization. Chen et al. (2019) explored the effect of removing soil background information on the inversion of nitrogen concentration in cotton plants using high spatial resolution UAV images. The authors concluded that the removal of soil background could improve the inversion accuracy. Zhang et al. (2018) used the binarized Ostu and Canny edge detection algorithms to mask thermal infrared images for soil background removal, pointing out that the removal was an effective way to improve the accuracy of crop moisture diagnosis. Liu et al. (2023) showed that the soil background present in UAV remote sensing images was an important factor affecting the estimation accuracy of crop leaf area index: by removing the soil background, the interference to the estimation of leaf area index could be reduced that would improve the estimation accuracy. Shu et al. (2021) comparatively analyzed the extent to which the background of UAV hyperspectral images affected the accuracy of leaf chlorophyll value estimation, and the study showed that the validation accuracy of the estimated model with the background removed was higher than that with the background. Wu et al (2022) pointed out that the soil background reduced the accuracy of leaf area index prediction for wheat. They showed that the soil background could be effectively removed using high-resolution UAV imagery, and consequently the prediction accuracy was significantly improved, increasing R^2 by about 0.27. Previous research results confirmed that culling soil background could effectively improve the diagnosis accuracy in crop nitrogen nutrition diagnosis, water stress diagnosis and leaf area index estimation, but little research has been reported on crop salt stress diagnosis. Therefore, further exploration of the combination of spectral features and texture features of UAV multi-spectral images for crop salt stress diagnosis, which is helpful to improve the practical application ability of UAV remote sensing technology in crop salt stress monitoring.

Considering the foregoing, taken alfalfa at the first flowering stage planted in saline and alkaline lands in arid oasis irrigation area of China as the research object, this paper extracted spectral reflectance to construct 15 vegetation indexes, and used gray level co-occurrence matrix (GLCM) to calculate eight image texture features based on UAV multispectral images and measured data from 2021-2023. The Canny edge detection algorithm was used to remove the soil background, and set T1 (vegetation index non-removed soil background), T2 (vegetation index+image texture features non-removed soil background), T3 (vegetation index removed soil background), T4 (vegetation index+image texture features removed soil background), as independent variables to construct alfalfa salt stress diagnosis model based on the support vector regression (SVR) algorithm by considering aboveground dry matter mass as a diagnosis indicator for salt stress in alfalfa. This paper aimed to: (1) explore whether the combination of UAV multispectral image texture features and vegetation index can improve the diagnostic accuracy of alfalfa salt stress, and the effect of soil background on the diagnostic accuracy of alfalfa salt stress. (2) compare and evaluate the accuracy of alfalfa salt stress diagnosis models under T1, T2, T3, and T4 schemes, and determine the optimal variable scheme and salt stress diagnosis model. (3) compare and evaluate the applicability and feasibility of the crop salt stress index (CSSI) constructed for diagnosing salt stress in alfalfa, and simplify the modeling process of crop salt stress diagnosis. To provide a new method for rapid, accurate, and large-scale diagnosis of crop salt stress conditions.

2. Materials and methods

2.1. Overview of the study area

The study area is located at Bianwan Farm in the Taolai River Basin, Gansu Province (Fig. 1(a)). This region is located at 98°20′~99°18′E, 39°10′~40°15′N, with temperate continental arid climate, dry and little rain, strong evaporation, average precipitation of 72.6 mm and average evaporation of 2184.0 mm. These characteristics make it a typical "no irrigation, no agriculture" area. The main crops are grain economic crops such as alfalfa, wheat and corn, which provide an important grain production base in the Hexi Corridor. This study selected alfalfa as the research object, and the alfalfa planted in the study area were all perennial purple clover varieties. The distribution of UAV operation area and soil sampling points is shown in Figure1 (b). The sampling area is 54,000 m^2, the soil texture is relatively uniform, the salt distribution is relatively uniform, and the spatial heterogeneity is small. According to the field survey, following the principle of uniform distribution, the location of sampling points is determined, and the location information of each sampling point is measured and recorded by hand-held GPS.

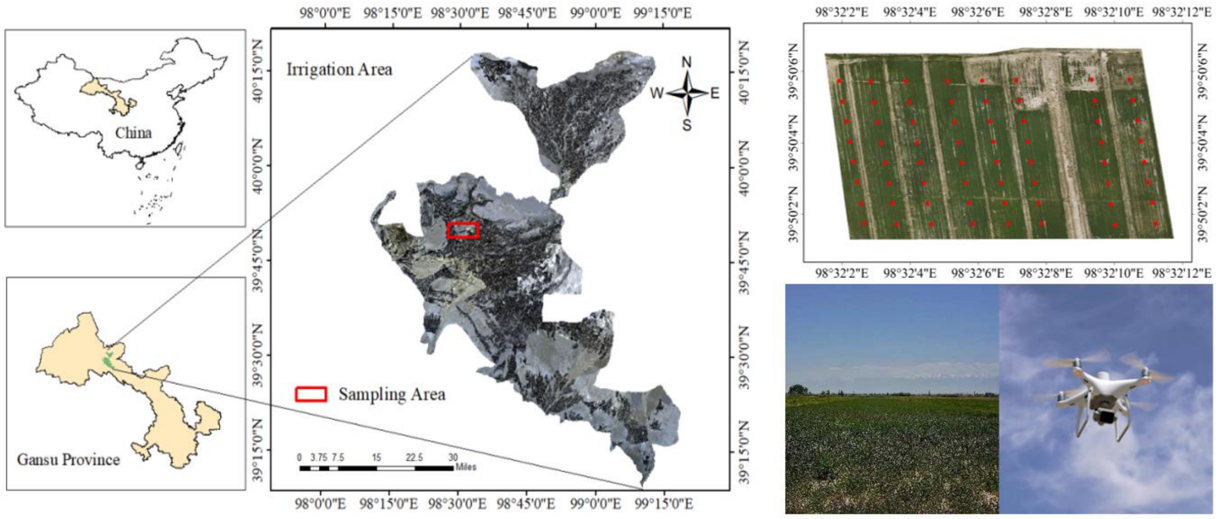

(a) Location of the study area **(b) Experimental plots and ground samplings**

Fig.1 Location of the study area,the field for the observation of an UAV and ground samplings

2.2. Data acquisition

2.2.1. UAV multispectral data acquisition and preprocessing

The UAV remote sensing platform used in this study is the DJI P4 multispectral version with a visible light camera and five multispectral cameras (blue 450 nm, green 560 nm, red 650 nm, near-infrared 840, and nmred edge 730 nm) (Table 1). The UAV multispectral remote sensing data were collected on May 21-23, 2021, May 25-27, 2022 and May 22-24, 2023, between 11:00-14:00 in the presence of clear and cloudless weather. The images were collected for three consecutive days each time, the image data of the sampling area was obtained by a single flight, and the sampling area is 54,000m^2. The UAV flight altitude was 75 m, with a ground resolution of 4.0 cm, and heading and side-to-side overlap rate set to 75%. Standard whiteboards were used for calibration. The collected multispectral images were imported into DJI Zhitu for image correction, cropping and other pre-processing.

Table.1 Parameters of the unmanned aerial multispectral remote sensing platform

Parameter	PTZ rotation range/°	Image resolution	Band and bandwidth/nm				
			B	G	R	RE	NIR
Size	-90° ～+30°	1600×1300	450nm±16	560nm±16	650nm±16	730nm±16	840nm±26

2.2.2. Field data acquisition

(1) Soil salinity measurement

The collection of soil salt samples was synchronized with the acquisition of UAV multispectral images. Sixty-four sampling points were evenly distributed in the sampling area, and soil samples from depths between 0-15 cm were collected using soil augers. The location information of each point was recorded. Each soil sample with weight equal to 30 g was collected into an aluminum box, oven-dried for 8 h, cooled and then ground and sieved (pore size 2 mm). Distilled water of volume equal to 150 ml was added to the sieved soil samples and stirred thoroughly, and after a few hours of standing, the conductivity of the soil solution was determined using a Raymag DJS-1C ($EC_{1:5}$, ms/cm). The soil salt content (SSC, %) was calculated according to the empirical formula SSC = 0.2882$EC_{1:5}$ + 0.0183 (Zhao et al., 2022).

(2) Determination of aboveground dry matter quality of alfalfa

Alfalfa aboveground biomass samples were collected simultaneously using canopy spectrometry. In this study, the data of the first flowering stage of alfalfa were selected for the diagnosis of salt stress in alfalfa. The main reason was that the first flowering stage was the key stage of the transition from vegetative growth to reproductive growth of alfalfa, which was most sensitive to salt stress, which can significantly reflect the effects of salt stress on its growth, development and physiological status (Yan et al., 2022; Xiong et al., 2017).The destructive sampling method was used to select four alfalfa plants with consistent and representative growth in a small area of each soil sampling point in the sampling area. The plants were heated at 105°C for 0.5 h, dried at 80°C to a constant mass, and weighed as dry mass (Yan et al., 2022).

2.3. Research methods

2.3.1 Technical route

Using the UAV multispectral remote sensing data from 2021 to 2023, this paper studied the diagnosis of alfalfa salt stress based on vegetation index and image texture features. The technical details were as follows: First, 15 vegetation indexes were constructed by extracting alfalfa spectral reflectance, and eight image texture features are calculated using GLCM. Alfalfa salt stress diagnosis models based on the support vector regression (SVR) algorithm were constructed with the vegetation indexes and image texture features as the independent variables. These models enable a comparative evaluation of the effect of increasing image texture features on the alfalfa salt stress diagnosis accuracy, and improved the salt stress diagnosis accuracy. Second, the Canny edge detection algorithm was used to remove the soil background, and comparatively analyzed the effect of soil background and reduced its interference on the diagnosis accuracy of crop salt stress. Last, the CSSI was constructed on this basis by using gray correlation analysis (GRA) for variable screening combined with the principal component analysis, which simplified the modeling process of crop salt stress diagnosis. This provided a new method for rapid, accurate and large-scale diagnosis of crop salt stress. Figure 2 shows the technology roadmap.

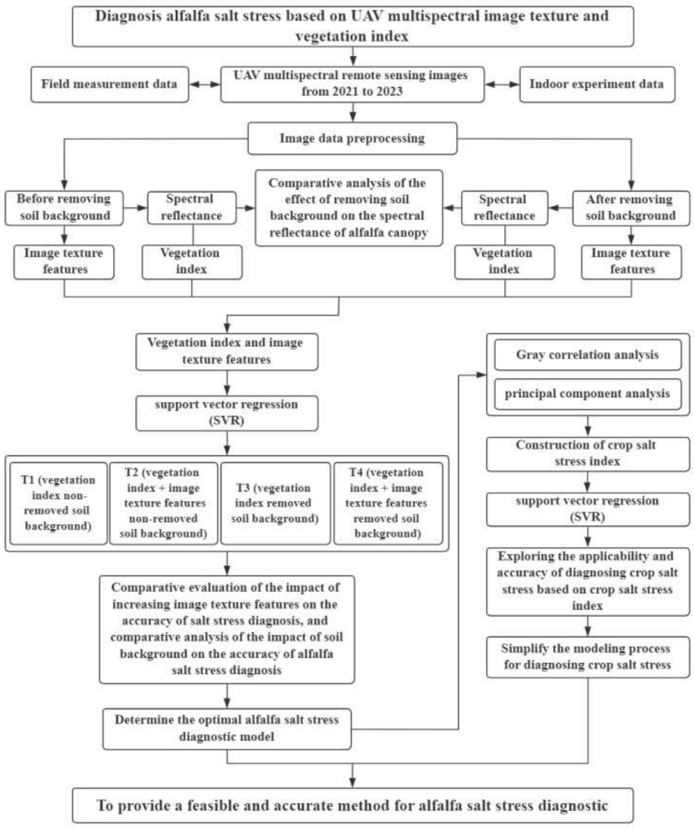

Fig.2 Sketch nap of the technical route

2.3.2. Construction and calculation of vegetation index

When the crop is subjected to salt stress, the canopy structure, leaf color, etc. will change, and the spectral reflectance of each band will also change. In order to enhance the interpretability of remote sensing images, this paper constructs 15 kinds of vegetation indexes as input parameters according to the spectral reflectance in different bands. Table 2 shows the corresponding calculation formula.

Table.2 Vegetation index and calculation formula

Vegetation index	Computing formula	Reference	Vegetation index	Computing formula	Reference
Optimized soil adjusted vegetation index (OSAVI)	1.16(NIR-R)/(NIR+R+0.16)	(Zhang et al., 2019)	Improved ratio index (MSR)	$(NIR/R-1)/(NIR/R+1)^{0.5}$	(Zhang et al., 2019)
Greenness normalized vegetation index (GNDVI)	(NIR-G)/(NIR+G)	(Mwinuka et al., 2022)	Canopy Salinity Response Vegetation Index (CRSI)	$[((NIR*R)-(G*B))/((NIR*R)+(G*B))]^{0.5}$	(Zhang et al., 2019)
Transformed vegetation index (TVI)	60(NIR-G)-100(R-G))	(Luo et al., 2022)	Improvement of chlorophyll absorption index (MCARI)	[(RE-R)-0.2(RE-G)]*(RE/R)	(Zhang et al., 2022)
Perpendicular vegetation index (PVI)	$(NIR-10.489R-6.604)/(10.489^2+1)^{0.5}$	(Luo et al., 2022)	Normalized pigment ratio index (NPCI)	(R-B)/(R+B)	(Zhang et al., 2022)
Ratio vegetation index (RVI)	NIR/R	(Luo et al., 2022)	Structure insensitive pigment vegetation index (SIPI)	(NIR-B)/(NIR+B)	(Zhang et al., 2022)
Normalized difference vegetation index (NDVI)	(NIR-R)/(NIR+R)	(Donovan et al., 2022)	Conversion chlorophyll absorption index (TCARI)	3[(RE-R)-0.2(RE-G)*(RE/R)]	(Zhang et al., 2022)
Enhanced vegetation index (EVI)	2.5(NIR-R)/(NIR+6R-7.5B+1)	(Luo et al., 2022)	Green chlorophyll index (GCI)	NIR/G-1	(Wu et al., 2012)
Differential vegetation index (DVI)	NIR-R	(Luo et al., 2022)			

Note: B, G, R, RE and NIR are the spectral reflectance at 450,560,650,730 and 840 nm, respectively.

2.3.3. Image texture feature calculation

The UAV multispectral remote sensing images contain not only spectral information, but also rich image texture information. This information can effectively indicate the physical properties of crop surface as it is an extremely important attribute of images. In this paper, image texture feature parameters are calculated by normalizing the GLCM, which is a statistical data-based image texture feature extraction method (Yue et al., 2019; Nguyen et al., 2023). In this paper, eight image texture feature parameters, namely mean, variance, homogeneity, contrast, dissimilarity, entropy, second moment and correlation, are used, which are calculated as shown in Table 3.

Table.3 Image texture feature parameters and calculation formula

Image texture feature parameters	Computing formula	Image texture feature parameters	Computing formula
Mean (MEA)	$MEA=\sum_{i}\sum_{j} i \cdot p(i,j)$	Dissimilarity (DIS)	$DIS=\sum_{n=0}^{N_g-1} n \begin{cases} \sum_{i=1}^{N_g}\sum_{j=1}^{N_g} p(i,j) \\ \lvert i-j\rvert = n \end{cases}$
Variance (VAR)	$VAR=\sum_{i}\sum_{j}(i-u)^2 p(i,j)$	Entropy (ENT)	$ENT=-\sum_{i}\sum_{j} p(i,j)\log(p(i,j))$
Homogeneity (HOM)	$HOM=\sum_{i}\sum_{j}\frac{1}{1+(i-j)^2} p(i,j)$	Second moment (SEC)	$SEC=\sum_{i}\sum_{j}[p(i,j)]^2$
Contrast (CON)	$CON=\sum_{n=0}^{N_g} n^2 \begin{cases} \sum_{i=1}^{N_g}\sum_{j=1}^{N_g} p(i,j) \\ \lvert i-j\rvert = n \end{cases}$	Correlation (COR)	$COR=\left[\sum_{i}\sum_{j}(i,j)p(i,j)-\mu_x\mu_y\right]/\sigma_x\sigma_y$

2.3.4. Canny edge detection algorithm

Edge detection is an important process in image preprocessing, which mainly utilizes the collection of pixel points with step change in image gray level, reflecting the abrupt change in DN value of the image.Canny edge detection algorithm has three decision criteria for edge test, which has better application effect for edge extraction of image, and Canny edge detection algorithm has greater advantage in the detection of gradient change in both horizontal and vertical direction (Canny, 1986; Maini et al., 2009).Canny edge detection algorithm is smoothed with the help of Gaussian filter and its Gaussian function is:

$$G(x,y)=\frac{1}{2\pi\sigma^2}\exp\left(-\frac{x^2+y^2}{2\sigma^2}\right) \tag{1}$$

where σ is the gaussian filter parameters.

2.3.5. Gray relational analysis

Gray correlation analysis (GRA) is a method that measures the correlation between various factors according to the degree of similarity or difference between the development trends of various factors (Wang et al., 2019). It is calculated as follows:

$$GRA=\frac{1}{m}\sum_{t=1}^{m}\beta[x_0(t),x_i(t)] \tag{2}$$

where $\beta[x_0(t),x_i(t)]=[\Delta(\min)+\rho\Delta(\max)]/[\Delta_{0i}(\mathrm{k})+\rho\Delta(\max)]$ and β is the discriminant coefficient, which is equal to 0.5.

2.3.6. Construction of crop salt stress index

To simplify the modeling process of crop salt stress diagnosis model, a comparative evaluation of the effects of adding image texture features and removing soil background on the diagnosis accuracy of alfalfa salt stress diagnosis is carried out. For this purpose, we adopt GRA to screen the vegetation index and image texture feature variables, and combine it with the principal component analysis method to propose the crop salt stress index (CSSI). The index can be calculated as follows:

$$CSSI=0.1[(NIR-B)/(NIR+B)]+0.373[(NIR-G)/(NIR+G)]+0.267[(NIR\cdot R-G\cdot R)/(NIR\cdot R+G\cdot R)]^{0.5}+0.26MEA \tag{3}$$

Where B, G, R, and NIR are the spectral reflectance at 450, 560, 650, and 840 nm wavelengths, respectively, and MEA is the mean value of the image texture features.

2.3.7. Construction and accuracy evaluation of salt stress diagnosis model

(1) Support vector regression algorithm

The support vector regression (SVR) algorithm is a supervised class of machine learning algorithms that realizes regression by constructing a hyperplane or a set of hyperplanes in a high-dimensional or infinite-dimensional space. The algorithm has the characteristics of strong generalization ability, simple structure, etc., and has obvious advantages in overcoming problems associated with a small number of samples, nonlinearities, etc. Thus, it can be used as an effective algorithm for constructing the diagnosis model of crop salt stress (Yan et al., 2022).

(2) Construction of salt stress diagnosis model

In this paper, In this paper, 70% of the sample set is divided into modeling set and 30% into validation set, where 44 samples are selected as the modeling set and the remaining 20 samples as the validation set. The vegetation index and image texture features are used as input independent variables, and the corresponding aboveground dry matter mass of alfalfa is the dependent variable. A total of four scenarios are set up to construct a SVR-based alfalfa salt stress diagnosis model, namely, T1 (vegetation index with soil background), T2 (vegetation index + image texture features with soil background), T3 (vegetation index without soil background) and T4 (vegetation index + image texture features without soil background).

(3) Accuracy evaluation

In this paper, the accuracies of the modeling and validation sets are evaluated using three indexes: the coefficient of determination (R^2), root mean square error (RMSE) and performance deviation ratio (RPD). The closer the value of R^2 is to 1, the closer the RMSE values is to 0, the larger the RPD. This indicates that the smaller the deviation between the predicted and measured values, the better the predictive ability of the diagnosis model (Zhang et al., 2019). These indexes can be calculated as follows:

$$R^2 = \sum_{i=1}^{n}(\hat{y}_i - \bar{y}_i)^2 \Big/ \sum_{i=1}^{n}(y_i - \bar{y}_i)^2 \tag{4}$$

$$RMSE = \sqrt{\sum_{i=1}^{n}(\hat{y}_i - y_i)^2 \Big/ n} \tag{5}$$

$$RPD = \frac{SD}{\text{RMSE}} \tag{6}$$

3. Results and analysis

3.1. Statistical analysis of soil salt content

The 64 soil samples used for salt content analysis were divided into three groups, namely, mild salinization soil (< 0.4%), moderate salinization soil (0.4% - 0.6%), and severe salinization soil (0.6% - 1.0%) (Wang et al., 2018). The statistical analysis results of soil salt content are shown in Table 4. The percentages of mild salinization soil, moderate salinization soil, and severe salinization soils were 35.0%, 57.0%, and 8.0%, respectively, and their coefficient of variation was 0.202, indicating that the salt content of the soil surface had moderately weak variability.

Table.4 The statistical analysis of soil salt content in alfalfa sampling sites

Sampling area	sampling time	Number of samples					Salt Content					
		Data set		Mild salinization soil	Moderate salinization soil	Severe salinization soil	Maximum (%)	Minimum (%)	Average (%)	Standard deviation	Variance	coefficient of variation
Alfalfa covered land	2021	Total sample	64	22	37	5	0.762	0.350	0.472	0.091	0.008	0.192
		Modeling set	44	11	28	5	0.762	0.350	0.493	0.095	0.009	0.193
		Verification set	20	11	9	0	0.583	0.376	0.427	0.059	0.004	0.137
	2022	Total sample	64	22	38	4	0.758	0.301	0.457	0.095	0.009	0.207
		Modeling set	44	14	26	4	0.758	0.301	0.475	0.102	0.011	0.214
		Verification set	20	8	12	0	0.582	0.331	0.417	0.061	0.004	0.145
	2023	Total sample	64	24	35	5	0.732	0.306	0.449	0.092	0.009	0.206
		Modeling set	44	14	25	5	0.732	0.306	0.464	0.100	0.010	0.215
		Verification set	20	10	10	0	0.599	0.323	0.415	0.062	0.004	0.149

3.2. Correlation analysis of alfalfa aboveground dry matter quality and soil salt content

Table 5 shows the correlation coefficients of alfalfa aboveground dry matter mass and soil salt content in 2021-2023 over the study area. It can be observed that the alfalfa aboveground dry matter mass and soil salt salinity are significantly correlated at the $p < 0.001$ level, and the absolute values of correlation coefficients are all greater than 0.86. This signifies a high correlation, indicating that the aboveground dry matter mass can better characterize the real situation of alfalfa subjected to salt stress, and can be used as a diagnosis index of alfalfa salt stress, this is consistent with reference Li et al. (2022) and reference Liu et al. (2021).

Table.5 Correlation between aboveground dry matter mass and soil salinity content

Sampling year	Correlation coefficient	Average	Standard deviation
2021	-0.875**	5.51	0.565
2022	-0.861**	5.62	0.367
2023	-0.883**	5.65	0.244

3.3. Correlation analysis between image texture features and aboveground dry matter quality

When the crop is subjected to salt stress, the canopy structure and leaf size will change, thus affecting the spectral characteristics of the crop canopy. These changes will be reflected in the image texture features. Table 6 shows the correlation coefficients between the image texture features and aboveground dry matter mass. Figure 3 shows the absolute values of the correlation coefficients between image texture features and aboveground dry matter mass at the first flowering stage of alfalfa from 2021 to 2023. As Table 6 and Fig. 3 show, image texture features are significantly correlated with aboveground dry matter mass at the $p < 0.01$ level (except for COR), which means that image texture features can be used to indicate salt stress conditions in alfalfa.

Table.6 Correlation coefficient between image texture features and aboveground dry matter quality

Textural features of the soil background not removed	Correlation coefficient			Textural features of the soil background removed	Correlation coefficient		
	2021	2022	2023		2021	2022	2023
Mean (MEA)	-0.566**	-0.559**	-0.607**	Mean (MEA)	0.633**	0.603**	0.656**
Variance (VAR)	-0.363**	-0.333**	-0.325**	Variance (VAR)	-0.535**	-0.445**	-0.498**
Homogeneity (HOM)	0.399**	0.327**	0.382**	Homogeneity (HOM)	-0.433**	-0.494**	-0.451**
Contrast (CON)	-0.432**	-0.444**	-0.426**	Contrast (CON)	-0.542**	-0.473**	-0.456**
Dissimilarity (DIS)	-0.335**	-0.462**	-0.356**	Dissimilarity (DIS)	-0.442**	-0.485**	-0.403**
Entropy (ENT)	-0.405**	-0.381**	-0.399**	Entropy (ENT)	0.502**	0.548**	0.531**
Second moment (SEC)	0.372**	-0.347**	0.302**	Second moment (SEC)	-0.542**	-0.581**	-0.478**
Correlation (COR)	-0.182*	-0.229*	-0.226*	Correlation (COR)	-0.242*	0.285*	0.271*

Note : * indicates significance test $p < 0.05$, * * indicates $p < 0.01$.

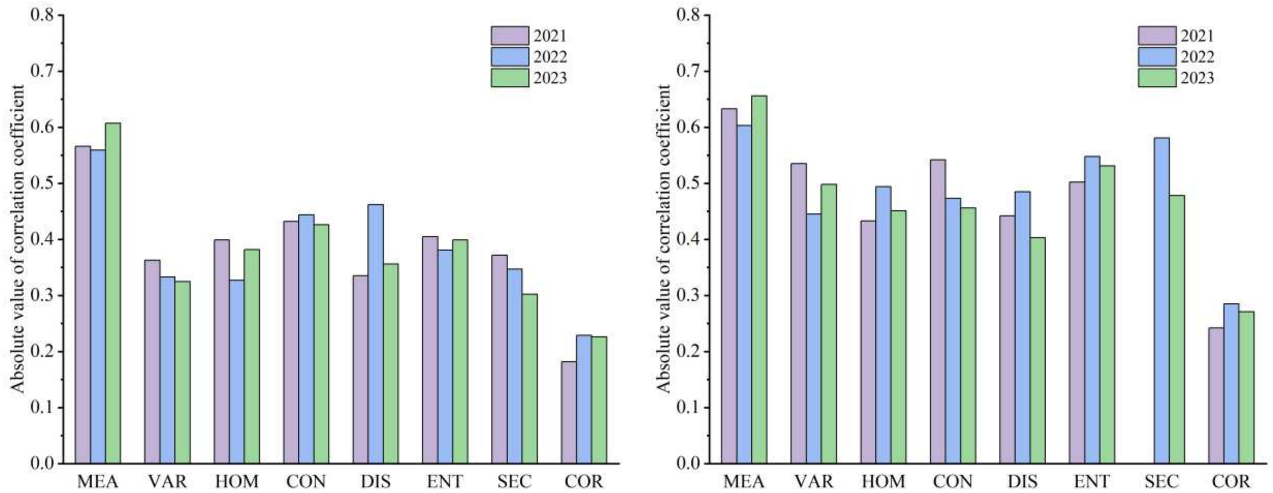

(a) Before removing the soil background (b) After removing the soil background

Fig.3 Absolute value of the correlation coefficient between image texture features and aboveground dry matter mass before and after removing soil background

3.4. Effects of removing soil background on alfalfa canopy reflectance

3.4.1. Soil background rejection

The coverage of alfalfa in the early flowering stage or under severe salt stress is low, and the obtained image is prone to the soil background interference problem. In this paper, the Canny edge detection algorithm is used to remove the soil background. It has certain advantages in the detection of gradient changes in the horizontal and vertical directions, and can effectively remove the soil background. First, the image is reclassified and aligned using ArcGIS and ENVI. Second, the raster to line and line to surface in ArcToolbox tool are used to close the edge line image. Last, the image is cropped using the ENVI software and the feature values are selected using the mask tool and the mask statistics function. This is followed by the application of the Canny edge detection algorithm to achieve soil background rejection (Fig. 4).

(a) 2021 image before soil background removal (b) 2022 image before soil background removal (c) 2023 image before soil background removal

(d) 2021 image after soil background removal (e) 2022 image after soil background removal (f) 2023 image after soil background removal

Fig.4 Soil background removal based on Canny edge detection algorithm

3.4.2. Effects of removing soil background on alfalfa canopy reflectance

Figure 5 shows the changes of alfalfa canopy reflectance before and after the removal of soil background based on the Canny edge detection algorithm. It can be observed that in the alfalfa primordial flowering stage, the canopy spectral reflectance in the red, green, blue, near-infrared and red-edge bands before the removal of soil background is greater than that after the removal of soil background. This behavior occurs because alfalfa in the early flowering stage or severe salt stress state has a low crop cover and there are more bare ground surfaces. The vast majority of these areas are directly illuminated by light, causing the soil background to affect the alfalfa canopy spectral reflectance.

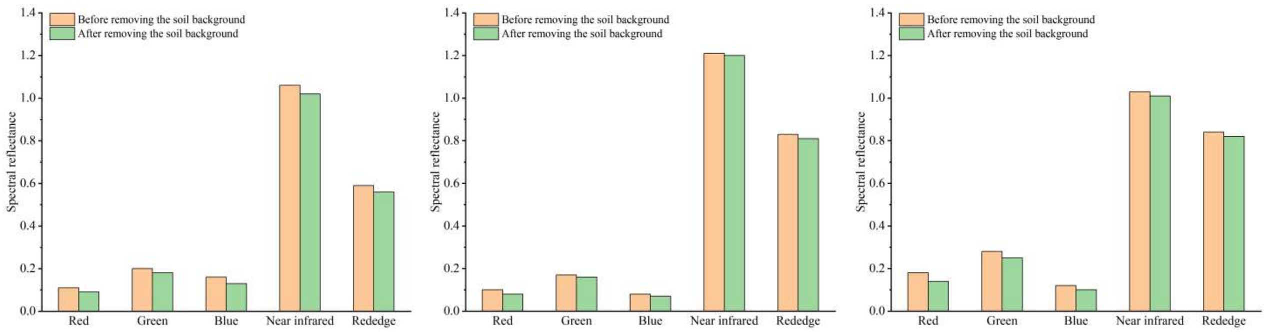

(a) Before and after removing the soil background in 2021 (b) Before and after removing the soil background in 2022 (c) Before and after removing the soil background in 2023

Fig.5 Variation of reflectance before and after removing soil background

3.5. Construction and evaluation of alfalfa salt stress diagnosis model based on spectroscopy image texture feature extraction and soil background removal

Table 7 shows the evaluation results of the proposed alfalfa salt stress diagnosis model based on UAV multispectral data and measured data from 2021-2023.

Table.7 Evaluation results of salt stress diagnosis models in alfalfa under different programs

Scheme	Year	Modeling set			Validation set		
		R^2	RMSE	RPD	R^2	RMSE	RPD
T1	2021	0.564	0.3766	1.4339	0.546	0.3899	1.4363
	2022	0.566	0.2769	1.4807	0.552	0.1524	2.2966
	2023	0.550	0.1939	1.7019	0.539	0.1500	1.8667
	Average	0.560	0.2825	1.5223	0.546	0.2308	1.7334
T2	2021	0.633	0.2925	1.4701	0.628	0.3871	1.4208
	2022	0.628	0.2489	1.5669	0.603	0.1385	2.3105
	2023	0.643	0.1506	2.0584	0.627	0.1139	2.3705
	Average	0.635	0.2307	1.6474	0.619	0.2132	1.7826

T3	2021	0.589	0.3486	1.4630	0.577	0.3137	1.5301
	2022	0.592	0.2772	1.6234	0.586	0.0857	2.5671
	2023	0.581	0.1665	2.1021	0.566	0.1132	1.5901
	Average	0.587	0.2641	1.6660	0.576	0.1709	1.6972
T4	2021	0.677	0.2667	1.4623	0.653	0.3536	1.4140
	2022	0.664	0.2325	1.8925	0.647	0.2661	1.7663
	2023	0.684	0.1436	2.2284	0.657	0.0851	1.7626
	Average	0.675	0.2143	1.7735	0.652	0.2349	1.5749

It can be observed that the modeling results of the alfalfa salt stress diagnosis model based on the T1 scheme show R^2 ranging from 0.550-0.566, RMSE ranging from 0.1939-0.3766, and RPD ranging from 1.4339-1.7019. The validation results show R^2 ranging from 0.539-0.552, RMSE ranging from 0.1500-0.3899, and RPD ranging from 1.4363-2.2966 (Figs. 6(a), 6(b), 6(c), 6(d), 6(e) and 6(f)). The modeling results of the alfalfa salt stress diagnosis model based on the T2 scheme have R^2 ranging from 0.628-0.643, RMSE ranging from 0.1506-0.2925, and RPD ranging from 1.4701-2.0584. The validation results show R^2 ranging from 0.603-0.628, RMSE ranging from 0.1139-0.3871, and RPD ranging from 1.4208-2.3705 (Figs. 6(g), 6(h), 6(i), 6(j), 6(k) and 6(l)). Compared with the results of the T1 scheme, the modeling and validation accuracy values of the alfalfa salt stress diagnosis model under the T2 scheme improve by 13.39% and 13.36%, respectively, indicating that the addition of image texture features can significantly improve the accuracy of alfalfa salt stress diagnosis.

As further shown in Table 7, the modeling results of the alfalfa salt stress diagnosis model based on the T4 scheme have R^2, RMSE and RPD ranging from 0.664-0.684, 0.1436-0.2667, and 1.4623-2.2284, respectively. The validation results have R^2, RMSE and RPD ranging from 0.647-0.657, 0.0851-0.3536, and 1.4140-1.7663, respectively (Figs. 6(s), 6(t), 6(u), 6(v), 6(w) and 6(x)). Thus, compared with the results based on the T2 scheme, the modeling and validation accuracies improve by 6.30% and 5.33%, respectively after the removal of soil background. This improvement indicates that the removal can effectively reduce the interference of soil background on the salt stress diagnosis process, and further improve its accuracy.

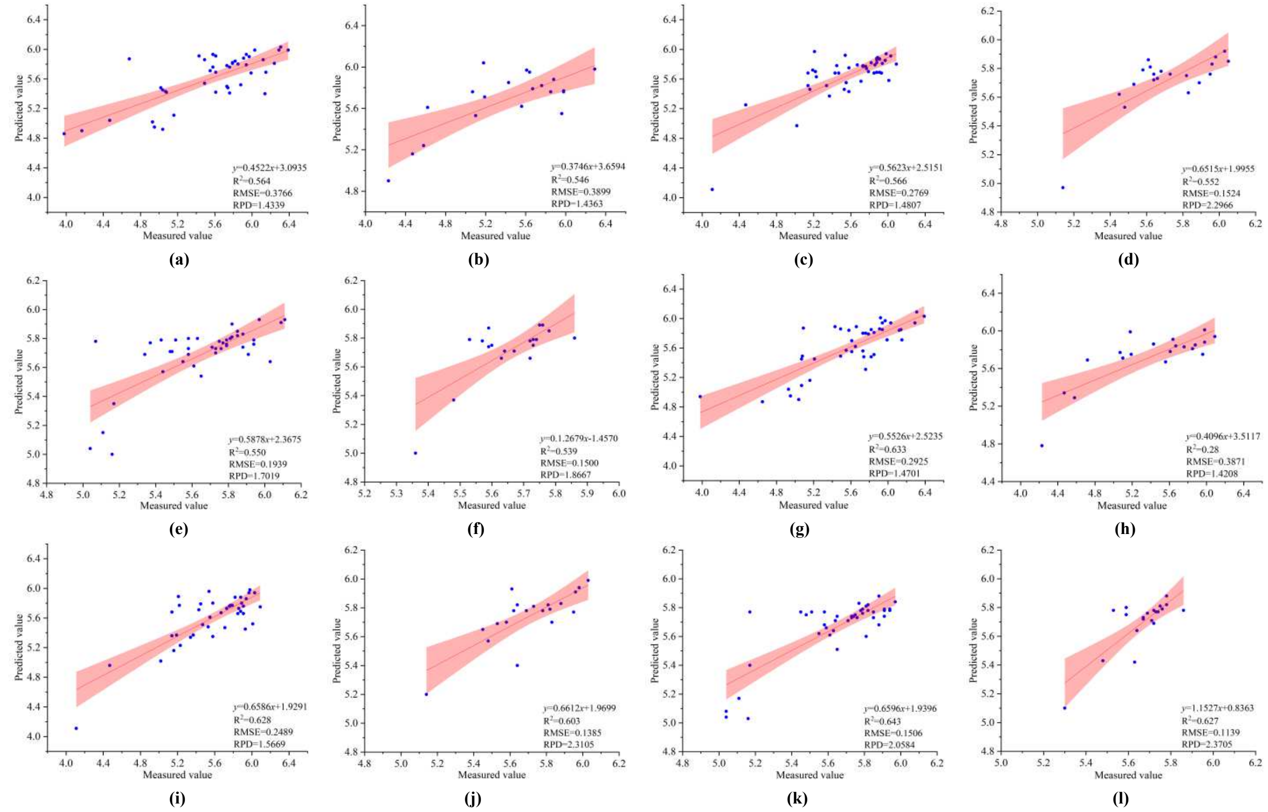

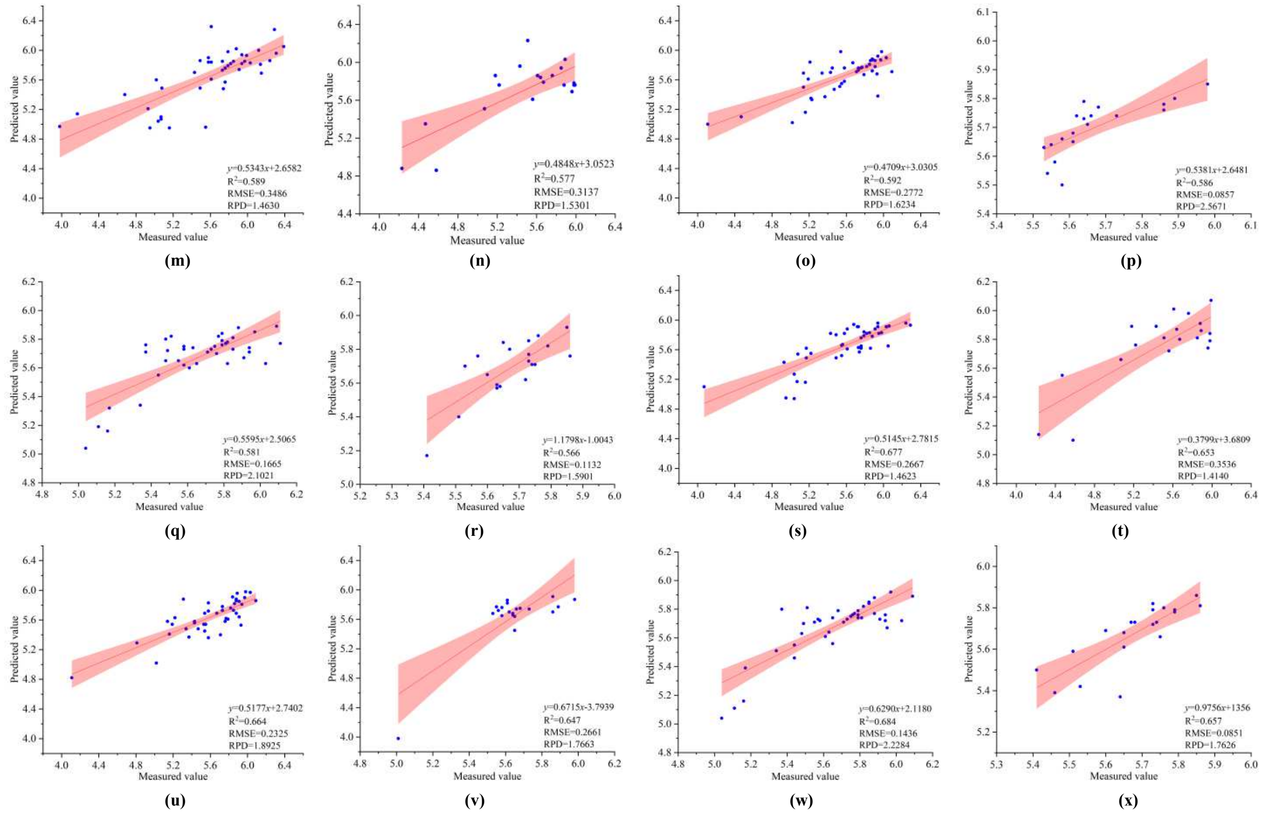

Fig.6 Diagnosis of salt stress in alfalfa under different programs. (a) T1 scheme modeling in 2021, (b) T1 scheme verification in 2021, (c) T1 scheme modeling in 2022, (d) T1 scheme verification in 2022, (e) T1 scheme modeling in 2023, (f) T1 scheme verification in 2023, (g) T2 scheme modeling in 2021, (h) T2 scheme verification in 2021, (i) T2 scheme modeling in 2022, (j) T2 scheme verification in 2022, (k) T2 scheme modeling in 2023, (l) T2 scheme verification in 2023, (m) T3 scheme modeling in 2021, (n) T3 scheme verification in 2021, (o) T3 scheme modeling in 2022, (p) T3 scheme verification in 2022, (q) T3 scheme modeling in 2023, (r) T3 scheme verification in 2023, (s) T4 scheme modeling in 2021, (t) T4 scheme verification in 2021, (u) T4 scheme modeling in 2022, (v) T4 scheme verification in 2022, (w) T4 scheme modeling in 2023, (x) T4 scheme verification in 2023.

3.6. Comprehensive evaluation of salt stress diagnosis models

Figure 7 shows the effects of the salt stress diagnosis models under different schemes were evaluated comparatively. It can be observed that the salt stress diagnosis models under different schemes have good robustness ($R_c^2/R_v^2>1.0$, R_c^2 is the modeling set coefficient of determination, and R_v^2 is the validation set coefficient of determination), indicating that the constructed salt stress diagnosis model can effectively diagnose the salt stress condition of alfalfa. In summary, it is shown that increasing image texture features as well as removing soil background can improve the diagnosis accuracy of crop salt stress. The alfalfa salt stress diagnosis model constructed based on T4 scheme is the best, with R^2, RMSE and RPD of 0.675, 0.2143 and 1.7735, respectively, over the modeling set, and R^2, RMSE and RPD of 0.652, 0.2349 and 1.5749, respectively, over the validation set.

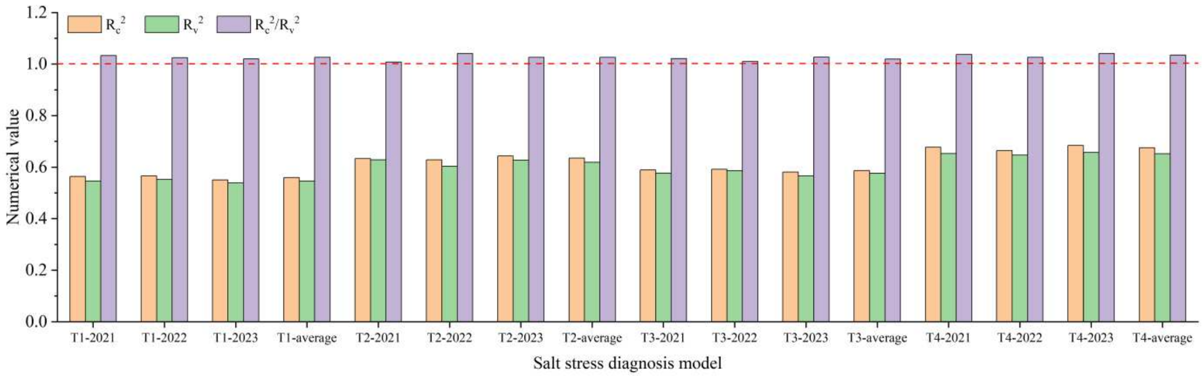

Fig.7 Modeling effects of salt stress diagnosis under different scenarios

3.7. Evaluation of alfalfa salt stress diagnosis based on CSSI

This paper uses the CSSI to compare and evaluate the applicability and accuracy of alfalfa salt stress diagnosis model under T1, T2, T3, and T4 schemes with UAV multispectral data and measured data from 2021 to 2023. The evaluation results are provided in Table 8.

Table.8 Evaluation results of alfalfa salt stress diagnosis model constructed based on CSSI

Scheme	Year	Modeling set			Validation set		
		R^2	RMSE	RPD	R^2	RMSE	RPD
T1	2021	0.546	0.3578	1.4626	0.533	0.3704	1.4506
	2022	0.551	0.2824	1.4955	0.542	0.1554	1.9521
	2023	0.549	0.1997	1.7274	0.541	0.1515	1.8853
	Average	0.548	0.2853	1.5527	0.538	0.2262	1.6987
T2	2021	0.564	0.3877	1.4186	0.549	0.4042	1.4102
	2022	0.573	0.3051	1.4422	0.565	0.1764	1.9274
	2023	0.569	0.1879	1.8627	0.553	0.1276	1.9592
	Average	0.569	0.2936	1.5329	0.556	0.2361	1.6097
T3	2021	0.552	0.3347	1.4776	0.545	0.3074	1.4995
	2022	0.561	0.2800	1.6721	0.553	0.1114	2.3104
	2023	0.558	0.1715	1.9129	0.547	0.1245	1.8286
	Average	0.557	0.2615	1.6910	0.548	0.1965	1.7227
T4	2021	0.593	0.2895	1.6235	0.577	0.3640	1.4286
	2022	0.586	0.1802	1.8868	0.562	0.1200	1.9167
	2023	0.598	0.1706	1.9343	0.581	0.1527	1.8991
	Average	0.592	0.2134	1.7804	0.576	0.2122	1.6491

Taking T2 and T4 schemes as examples, it can be observed from Table 8 that under the T2 scheme, the modeling results of the alfalfa salt stress diagnosis model based on the CSSI have R^2, RMSE and RPD ranging from 0.564-0.573, 0.1879-0.3877, and 1.4186-1.8627, respectively. The validation results have R^2, RMSE and RPD ranging from 0.549-0.565, 0.1276-0.4042, and 1.4102-1.9592, respectively (Figs. 8(a), 8(b), 8(c), 8(d), 8(e) and 8(f)). Compared with the T2 scheme, the modeling and validation accuracies of the alfalfa salt stress diagnosis model based on the CSSI under the T4 scheme is further improved: the modeling results exhibit R^2, RMSE and RPD ranging from 0.586-0.598, 0.1706-0.2895, and 1.6235-1.9343, respectively. The validation results exhibit R^2, RMSE and RPD ranging from 0.562-0.581, 0.1527-0.3640, and 1.4286-1.9167, respectively (Figs. 8(g), 8(h), 8(i), 8(j), 8(k) and 8(l)).

In summary, the alfalfa salt stress diagnosis model based on the CSSI has high diagnosis accuracies under T2 and T4 scenarios. Thus, the CSSI can be used as a new index to diagnose salt stress condition.

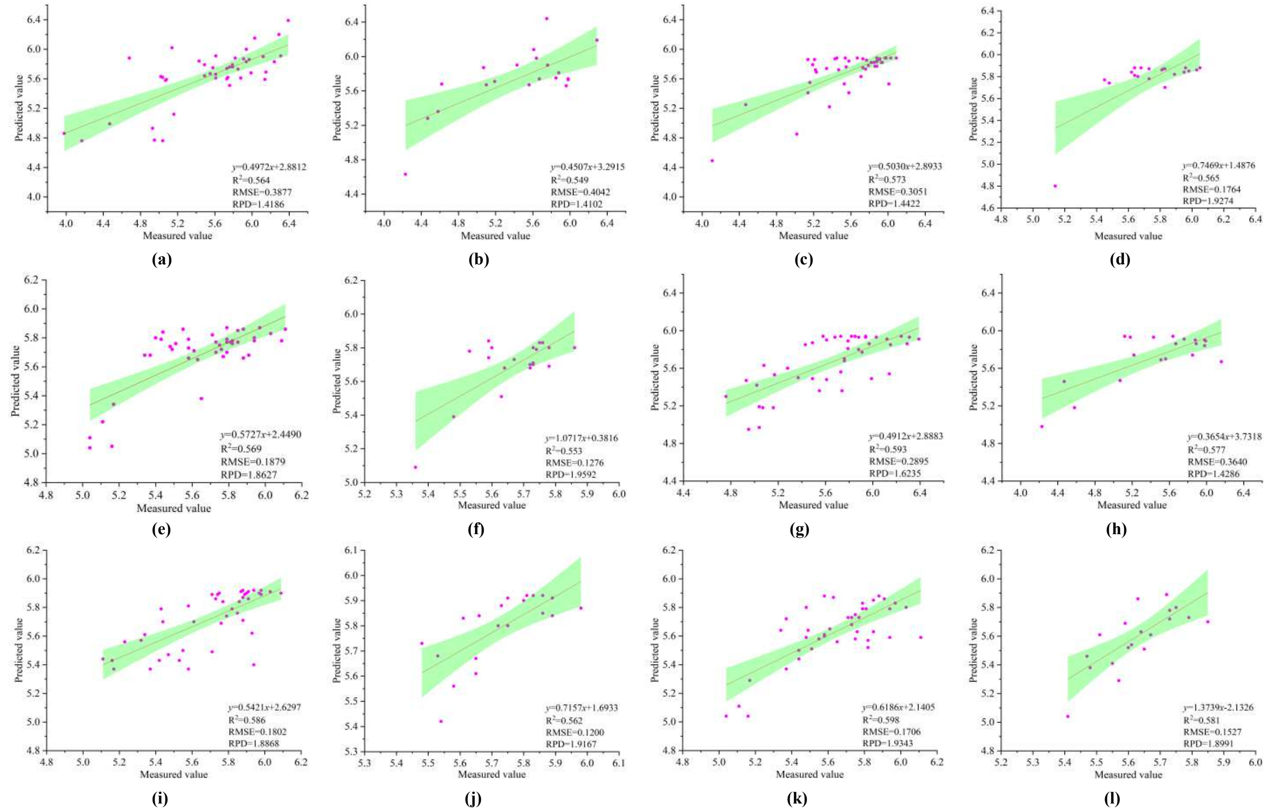

Fig.8 Diagnosis results of alfalfa salt stress under different strategies based on CSSCI. (a) T2 scheme modeling in 2021, (b) T2 scheme verification in 2021, (c) T2 scheme modeling in 2022, (d) T2 scheme verification in 2022, (e) T2 scheme modeling in 2023, (f) T2 scheme verification in 2023, (g) T4 scheme modeling in 2021, (h) T4 scheme verification in 2021, (i) T4 scheme modeling in 2022, (j) T4 scheme verification in 2022, (k) T4 scheme modeling in 2023, (l) T4 scheme verification in 2023.

4. Discussion

This work utilizes UAV remote sensing technology to obtain rich spectral and image texture information. Using this information, it proposes an alfalfa salt stress diagnosis model based on vegetation index and image texture features, significantly improving the salt stress diagnosis accuracy. By removing the soil background, crop canopy spectral information is optimized, reducing the interference of soil background on crop salt stress diagnosis and further improving the alfalfa salt stress diagnosis accuracy. At the same time, the constructed CSSI simplifies the modeling process of crop salt stress diagnosis, which can effectively diagnose the salt stress status of alfalfa. This study provides a new method for rapid, accurate and large-scale diagnosis of crop salt stress conditions.

It has been shown that canopy images can be used as an effective tool for diagnosing soil salt stress, not only reflecting the physiological changes of crops, but also revealing the dynamic characteristics of their spatial structure (Habure et al., 2020; Shi et al., 2023). The vegetation index constructed by extracting the spectral reflectance of the crop canopy can effectively diagnose the growth condition of crops, which can provide a theoretical basis for soil management and salt stress monitoring in precision agriculture. (Zhang et al., 2021; Zhang et al., 2023). Ma et al., (2021) and Zhang et al., (2021) confirmed the efficacy of using vegetation index for estimating cotton leaf area index and wheat growth parameters. The authors pointed out that the vegetation index could quantitatively monitor the growth status of crops through differences in crop and soil backgrounds within different bands. Although the monitoring of crop growth status based on vegetation index was proved to be feasible, its diagnosis accuracy was relatively low. The monitoring accuracy could be effectively improved by adding image texture features (Zhou et al., 2021; Zhao et al., 2023; Ma et al., 2022; Qiao et al., 2022). Freitas et al. (2022) showed that the R^2 of the aboveground biomass estimation model based on vegetation index was only 0.60, and it could be improved to 0.70 by adding image texture features.

Similarly, Zhou et al. (2021) pointed out that the addition of image texture features improved the diagnosis accuracy of water stress diagnosis in winter wheat by 24% compared to that without image texture features. This study also confirms that adding image texture features can significantly improve the accuracy of alfalfa salt stress diagnosis. The modeling and validation accuracies improve by 13.39% and 13.36%, respectively, compared to those without any image texture features. This improvement is possible mainly because image texture can quantify the changes in pixel values between adjacent pixels, effectively reflecting the changes in physical properties of crop surfaces. Adding image texture features will improve the correlation of vegetation index and image texture features with crop growth parameters, thereby improving the monitoring accuracy of crop growth status.

Meanwhile, the presence of soil background interference in the obtained UAV multispectral remote sensing images can affect the monitoring accuracy of crop growth status (Liu et al., 2023; Wu et al., 2022; Ma et al., 2022; Zhang et al., 2021). Chen et al. (2019) pointed out that the modeling coefficients of determination of the inversion model of plant nitrogen concentration were 0.33 and 0.38 before and after the removal of soil background, respectively. This difference confirmed that the removal of soil background could improve the accuracy of the inversion of nitrogen concentration in cotton plants. Shu et al (2021) analyzed the accuracy of chlorophyll value estimation before and after removal of soil background. The R^2 of the estimation model increased by 60.87% after removing the soil background. This study also confirms that removing soil background could reduce its interference in the establishment of crop salt stress diagnosis models. Compared with the results without any soil background removal, the modeling and validation accuracies improve by 6.30% and 5.33%, respectively. This improvement is possible because removing soil background could reduce the interference of soil background, optimize crop canopy spectral information, and thus improve the crop salt stress diagnosis accuracy. However, Xiang et al. (2023) pointed out that removing soil background could reduce the soil salinity inversion accuracy, which was contrary to the research results presented in (Chen et al., 2019), (Yan et al., 2022) and this paper. This difference may be due to the different effects of soil background on the spectral characteristics of different crop canopies, resulting in certain differences between the extracted spectral information and image texture information. Removal of soil background will reduce the correlation between the vegetation index and image texture features of sunflowers, corn and soil salt content.

Crop canopy image provides an efficient remote sensing method for soil salinity monitoring, and the relationship between soil salinity and crop growth can be revealed by extracting and analyzing spectral and texture features. In the follow-up study, further crop salt stress diagnosis research will be carried out from multi-scale and multi-dimension to enhance the robustness of the model, and improve the diagnostic accuracy and generalization ability. So as to construct a crop salt stress diagnosis model with higher accuracy and stronger applicability.

5. Conclusion

This paper considered alfalfa in saline alkali irrigated areas of arid oases in China as the research object. Based on UAV multispectral images and measured data from 2021-2023, the spectral reflectance of alfalfa was extracted to construct 15 vegetation indexes. A total of eight image texture features were obtained by GLCM. The Canny edge detection algorithm was used to eliminate the soil background, and the diagnosis of alfalfa salt stress based on vegetation index and image texture features was carried out. The main conclusions are as follows:

(1) The UAV multispectral image texture features had a good application effect in alfalfa salt stress diagnosis, and the addition of these features could significantly improve the salt stress diagnosis accuracy. The modeling and validation accuracies improved by 13.39% and 13.36%, respectively, compared with those without image texture features, thus providing a feasible and accurate method for alfalfa salt stress diagnosis.

(2) Removing the soil background could further improve the salt stress diagnosis accuracy. The modeling and verification accuracies increased by 6.30% and 5.33%, respectively, compared with those in the presence of soil background. The accuracy of alfalfa salt stress diagnosis model based on vegetation index and image texture features

after the removal of soil background was the highest. The modeling set R^2, RMSE and RPD were 0.675, 0.2143 and 1.7735, respectively and the validation set R^2, RMSE and RPD were 0.652, 0.2349 and 1.5749, respectively.

(3) The constructed CSSI simplified the modeling process of crop salt stress diagnosis, which could result in effective diagnosis of the salt stress status of alfalfa. The modeling set R^2, RMSE and RPD of alfalfa salt stress diagnosis model based on the CSSI were 0.592, 0.2134 and 1.7804, respectively, and the validation set R^2, RMSE and RPD were 0.576, 0.2122 and 1.6491, respectively.

Acknowledgment We thank the Taolai River Basin Water Resources Utilization Center, Gansu Provincial Department of Water Resources for providing the vector files of the study area. We are especially grateful to the reviewers and editors for appraising our manuscript and for offering instructive comments.

Author Contributions All authors contributed to the study conception and design. **Hong Ma:** Investigation, Data curation, Writing - original draft, Writing - review & editing, Funding acquisition. **Wenju Zhao:** Writing - review & editing, Supervision, Funding acquisition. **Haiying Yu:** Writing - review & editing, Investigation, Validation. **Pengtao Yang:** Investigation, Validation. **Faqi Yang:** Investigation, Validation. **Zongli Li:** Investigation, Validation.

Funding This work was supported by The National Natural Science Foundation of China (52379042), Gansu Province College Teachers' Innovation Fund Program (2024B-344), and Key Projects of Jiuquan Vocational and Technical College (2023XJZXM01).

Data Availability All data generated or analysed during this study are included in this published article. However, the corresponding author can provide more detailed information on this current study at rea sonable request.

Declarations

Competing Interests All authors certify that they have no affiliations with or involvement in any organization or entity with any financial or non-financial interest in the subject matter or materials discussed in this manuscript.

References

Aktas A, Üstündağ B B (2020) Soil moisture monitoring of the plant root zone by using phenology as context in remote sensing. IEEE J-STARS. 13, 6051-6063. https://doi.org/10.1109/jstars.2020.3021990.

Almeida-Ñauñay A F, Tarquis A M, López-Herrera J, Pérez-Martín E, Pancorbo J L, Raya-Sereno M D, Quemada M (2023) Optimization of soil background removal to improve the prediction of wheat traits with UAV imagery. Comput. Electron. Agric. 205, 107559. https://doi.org/10.1016/j.compag.2022.107559.

Behera T K, Krishna R, Ansari W A, Aamir M, Kumar P, Kashyap S P, Pandey S, Kole C (2022) Approaches involved in the vegetable crops salt stress tolerance improvement: Present status and way ahead. Front. Plant Sci. 12, 787292. https://doi.org/10.3389/fpls.2021.787292.

Chen S, Song C, Mao X, Shang S (2022) Modeling response of spring wheat yield to soil water and salt contents and its application in scheduling brackish water irrigation. Comput. Electron. Agric. 200, 107216. https://doi.org/10.1016/j.compag.2022.107216.

Chen P, Liang F (2019) Cotton nitrogen nutrition diagnosis based on spectrum and texture feature of images from low altitude unmanned aerial vehicle. Scientia Agric. Sin. 52(13), 2220-2229. https://doi.org/10.3864/j.issn.0578-1752.2019.13.003.

Canny J (1986) A computational approach to edge detection. IEEE Trans. Pattern Anal. Mach. Intell. PAMI-8(6): 679-698. https://doi.org/10.1109/TPAMI.1986.4767851.

Donovan G H, Gatziolis D, Derrien M, Michael Y L, Prestemon J P, Douwes J (2022) Shortcomings of the normalized difference vegetation index as an exposure metric. Nat. Plants. 8(6), 617-622. https://doi.org/10.1038/s41477-022-01170-6.

Feng Z, Guan H, Yang T, He L, Duan J, Song L, Wang H, Feng W (2023) Estimating the canopy chlorophyll content of winter wheat under nitrogen deficiency and powdery mildew stress using machine learning. Comput. Electron. Agric. 211, 107989.

https://doi.org/10.1016/j.compag.2023.107989.

Freitas R G, Pereira F R, Dos Reis A A, Magalhães P S, Figueiredo G K, Do Amaral L R (2022) Estimating pasture aboveground biomass under an integrated crop-livestock system based on spectral and texture measures derived from UAV images. Comput. Electron. Agric. 198, 107122. https://doi.org/10.1016/j.compag.2022.107122.

Gupta S, Schillaci M, Walker R, Smith P M C, Watt M, Roessner U (2021) Alleviation of salinity stress in plants by endophytic plant-fungal symbiosis: Current knowledge, perspectives and future directions. Plant Soil. 461, 219-244. https://doi.org/10.1007/s11104-020-04618-w.

Habure, Zhang B, Li S, Peng Z, Han N, Liu L (2020) Estimating Water Content of Winter Wheat Canopy Based on Its Spectral Characteristics. Journal of Irrigation and Drainage. 37(10): 9-15. https://doi:10.13522/j.cnki.ggps.20180021.

Ilniyaz O, Du Q, Shen H, He W, Feng L, Azadi H, Kurban A, Chen X (2023) Leaf area index estimation of pergola-trained vineyards in arid regions using classical and deep learning methods based on UAV-based RGB images. Comput. Electron. Agric. 207, 107723. https://doi.org/10.1016/j.compag.2023.107723.

Kawamura K, Asai H, Yasuda T, Soisouvanh P, Phongchanmixay S (2021) Discriminating crops/weeds in an upland rice field from UAV images with the SLIC-RF algorithm. Plant Prod. Sci. 24(2), 198-215. https://doi.org/10.1080/1343943x.2020.1829490.

Li H, Yang G, Long H, Feng H, Xu B, Zhao C (2023) Estimating characteristic coefficient of vertical leaf nitrogen profile within wheat canopy from spectral reflectance. Comput. Electron. Agric. 206, 107652. https://doi.org/10.1016/j.compag.2023.107652.

Liu Y, Feng H, Yue J, Jin X, Li Z, Yang G (2022) Estimation of potato above-ground biomass based on unmanned aerial vehicle red-green-blue images with different texture features and crop height. Front. Plant Sci. 13, 938216. https://doi.org/10.3389/fpls.2022.938216.

Liu S, Jin X, Bai Y, Wu W, Cui N, Cheng M, Liu Y, Meng L, Jia X, Nie C, Yin D (2023) UAV multispectral images for accurate estimation of the maize LAI considering the effect of soil background. Int. J Appl. Earth Obs. 121, 103383. https://doi.org/10.1016/j.jag.2023.103383.

Luo D, Gao Y, Wang Y, Shi Y, Chen S, Ding Z, Fan K (2022) Using UAV image data to monitor the effects of different nitrogen application rates on tea quality. J. Sci. Food Agric. 102(4), 1540-1549. https://doi.org/10.1002/jsfa.11489.

Li S, Lu X, Zheng W, He S, Lin H, Luo W, Lin Y (2022) Responses of growth and physiological indicators and canopy spectra of suaeda salsato water-salt stresses. Transactions of Oceanology and Limnology. 44(3): 31-40. https:// doi.org/10.13984/j. cnki. cn37-1141.2022.03.005.

Liu Y,Wu W, Yao Z, Ju C, Liu T, Sun C (2021) Advances on the effects of salt stress on crop growth and its monitoring technology. Journal of Chinese Agricultural Mechanization. 42(6):208-214. https://doi.org/10.13733/j.jcam.issn.2095-5553.2021.06.31.

Mandal D, Ratha D, Bhattacharya A, Kumar V, McNairn H, Rao Y S, Frery A C (2020) A radar vegetation index for crop monitoring using compact polarimetric SAR data. IEEE Trans. Geosci. Remote Sens. 58(9), 6321-6335. https://doi.org/ 10.1109/tgrs.2020.2976661.

Maes W H, Steppe K (2019) Perspectives for remote sensing with unmanned aerial vehicles in precision agriculture. Trends Plant Sci. 24(2), 152-164. https://doi.org/10.1016/j.tplants.2018.11.007.

Maimaitijiang M, Sagan V, Sidike P, Hartling S, Esposito F, Fritschi F B (2020) Soybean yield prediction from UAV using multimodal data fusion and deep learning. Remote Sens. Environ. 237, 111599. https://doi.org/10.1016/j.rse.2019.111599.

Ma Y, Zhang Q, Yi X, Ma L, Zhang L, Huang C, Zhang Z, Lv X (2021) Estimation of cotton leaf area index (LAI) based on spectral transformation and vegetation index. Remote Sens. 14(1), 136. https://doi.org/10.3390/rs14010136.

Mwinuka P R, Mourice S K, Mbungu W B, Mbilinyi B P, Tumbo S D, Schmitter P (2022) UAV-based multispectral vegetation indices for assessing the interactive effects of water and nitrogen in irrigated horticultural crops production under tropical sub-humid conditions: A case of African eggplant. Agr. Water Manage. 266, 107516. https://doi.org/10.1016/ j.agwat.2022. 107516.

Ma Y, Ma L, Zhang Q, Huang C, Yi X, Chen X, Hou T, Lv X, Zhang Z (2022) Cotton yield estimation based on vegetation indices and texture features derived from RGB image. Front. Plant Sci. 13, 925986. https://doi.org/10.3389/fpls.2022.925986.

Maini R, Aggarwal H (2009) Study and comparison of various image edge detection techniques. IET Image Processing. 3(1): 1-11.

Nguyen C, Sagan V, Skobalski J, Severo J I (2023) Early Detection of Wheat Yellow Rust Disease and Its Impact on Terminal Yield with Multi-Spectral UAV-Imagery. Remote Sens. 15(13), 3301. https://doi.org/10.3390/rs15133301.

Pan Y, Zhou R, Zhang J, Guo W, Yu M, Guo C, Yao X, Cheng T, Zhu Y, Cao W, Tian Y (2023) A new spectral index for estimation of wheat canopy chlorophyll density: considering background interference and view zenith angle effect. Precis. Agric. 1-28. https://doi.org/10.1007/s11119-023-10032-w.

Qi H, Wu Z, Zhang L, Li J, Zhou J, Jun Z, Zhu B (2021) Monitoring of peanut leaves chlorophyll content based on drone-based multispectral image feature extraction. Comput. Electron. Agric. 187, 106292. https://doi.org/10.1016/j.compag.2021.106292.

Qiao L, Zhao R, Tang W, An L, Sun H, Li M, Wang N, Liu Y, Liu G (2022) Estimating maize LAI by exploring deep features of vegetation index map from UAV multispectral images. Field Crop Res. 289, 108739. https://doi.org/10.1016/j.fcr.2022.108739.

Ryu J H, Jeong H, Cho J (2020) Performances of vegetation indices on paddy rice at elevated air temperature, heat stress, and herbicide damage. Remote Sens. 12(16), 2654. https://doi.org/10.3390/rs12162654.

Steinhorst L, Kudla J (2019) How plants perceive salt. Nature, 572: 318-320. https://doi.org/10.1038/d41586-019-02289-x.

Schut A G, Traore P C S, Blaes X,, De By R A (2018) Assessing yield and fertilizer response in heterogeneous smallholder fields with UAVs and satellites. Field Crop Res. 221, 98-107. https://doi.org/10.1016/j.fcr.2018.02.018.

Shen P, Ma X, Guan H, Zhang T (2023) Calculation method of wilting index based on fractal dimension of multispectral images for the soybean canopy. Comput. Electron. Agric. 206, 107656. https://doi.org/10.1016/j.compag.2023.107656.

Sun X, Yang Z, Su P, Wei K, Wang Z, Yang C, Wang C, Qin M, Xiao L, Yang W, Zhang M, Song X, Feng M (2023) Non-destructive monitoring of maize LAI by fusing UAV spectral and textural features. Front. Plant Sci. 14, 1158837. https://doi.org/10.3389/fpls.2023.1158837.

Shi X, Song J, Wang H, Lv X, Tian T, Wang J, Li W, Zhong M, Jiang M (2023) Improving the monitoring of root zone soil salinity under vegetation cover conditions by combining canopy spectral information and crop growth parameters. Front. Plant Sci. 14: 1171594. https://doi.org/10.3389/fpls.2023.1171594.

Shu M, Zuo J, Shen M, Yin P, Wang M, Yang X, Tang J, Li B, Ma Y (2021) Improving the estimation accuracy of SPAD values for maize leaves by removing UAV hyperspectral image backgrounds. Int. J Remote Sens. 42(15), 5862-5881. https://doi.org/10.1080/01431161.2021.1931539.

Tian Y, Huang H, Zhou G, Zhang Q, Tao J, Zhang Y, Lin J (2021) Aboveground mangrove biomass estimation in Beibu Gulf using machine learning and UAV remote sensing. Remote Sens. Environ. 781, 146816. https://doi.org/10.1016/j.scitotenv.2021.146816.

Wu S, Deng L, Guo L, Wu Y (2022) Wheat leaf area index prediction using data fusion based on high-resolution unmanned aerial vehicle imagery. Plant Methods. 18(1), 1-16. https://doi.org/10.1186/s13007-022-00899-7.

Wang H, Chen Y, Zhang Z, Chen H, Li X, Wang M, Chai H (2019) Quantitatively estimating main soil water-soluble salt ions content based on Visible-near infrared wavelength selected using GC, SR and VIP. PeerJ. 7, e6310. https://doi.org/10.7717/peerj.6310.

Wu C, Niu Z, Gao S (2012) The potential of the satellite derived green chlorophyll index for estimating midday light use efficiency in maize, coniferous forest and grassland. Ecol. Indic. 14(1), 66-73. https://doi.org/10.1016/j.ecolind.2011.08.018.

Xiang Y, Li W, Tai X, An J, Wang X, Chen J (2023) Inversion of soil salt content based on texture feature and vegetation index of UAV remote sensing images. Trans. Chin. Soc. Agric. Mach. 54(8):201-210. https://doi.org/10.6041/j.issn.1000-1298.2023.08.019.

Xiong J, Sun Y, Yang Q, Tian H, Zhang H, Liu Y, Chen M (2017) Proteomic analysis of early salt stress responsive proteins in alfalfa roots and shoots. Proteome Sci. 15: 1-19. https://doi.org/10.1186/s12953-017-0127-z.

Yue J, Yang H, Yang G, Fu Y, Wang H, Zhou C (2023) Estimating vertically growing crop above-ground biomass based on UAV remote sensing. Comput. Electron. Agric. 205, 107627. https://doi.org/10.1016/j.compag.2023.107627.

Yue J, Yang G, Tian Q, Feng H, Xu K, Zhou C (2019) Estimate of winter-wheat above-ground biomass based on UAV ultrahigh-ground-resolution image textures and vegetation indices. ISPRS J Photogramm. 150, 226-244. https://doi.org/10.1016/ j.isprsjprs. 2019.02.022.

Yuan W, Meng Y, Li Y, Ji Z, Kong Q, Gao R, Su Z (2023) Research on rice leaf area index estimation based on fusion of texture and spectral information. Comput. Electron. Agric. 211, 108016. https://doi.org/10.1016/j.compag.2023.108016.

Yan H, Zhuo Y, Li M, Wang Y, Guo H, Wang J, Li C, Ding F (2022) Alfalfa yield prediction using machine learning and UAV multispectral remote sensing. Transactions of the CSAE. 38(11): 64-71. https://doi.org/10.11975/j.issn.1002-6819.2022.11.007.

Zhao W, Zhou C, Zhou C, Ma H, Wang Z (2022) Soil salinity inversion model of oasis in arid area based on UAV multispectral remote sensing. Remote Sensing, 14(8), 1804. https://doi.org/10.3390/rs14081804.

Zhang C, Liu J, Shang J, Dong T, Tang M, Feng S, Cai H (2021) Improving winter wheat biomass and evapotranspiration simulation by assimilating leaf area index from spectral information into a crop growth model. Agr. Water Manage. 255, 107057. https://doi.org/10.1016/j.agwat.2021.107057.

Zhang Y, Han W, Zhang H, Niu X, Shao G (2023) Evaluating soil moisture content under maize coverage using UAV multimodal data by machine learning algorithms. J. Hydrolo. 617, 129086. https://doi.org/10.1016/j.jhydrol.2023.129086.

Zhang J, Qiu X, Wu Y, Zhu Y, Cao Q, Liu X, Cao W (2021) Combining texture, color, and vegetation indices from fixed-wing UAS imagery to estimate wheat growth parameters using multivariate regression methods. Comput. Electron. Agric. 185, 106138. https://doi.org/10.1016/j.compag.2021.106138.

Zhou Y, Lao C, Yang Y, Zhang Z, Chen H, Chen Y, Chen J, Ning J, Yang N (2021) Diagnosis of winter-wheat water stress based on UAV-borne multispectral image texture and vegetation indices. Agr. Water Manage. 256, 107076. https://doi.org/10.1016/j.agwat.2021.107076.

Zhao W, Ma F, Yu H, Li Z (2023) Inversion Model of Salt Content in Alfalfa-Covered Soil Based on a Combination of UAV Spectral and Texture Information. Agric. 13(8), 1530. https://doi.org/10.3390/agriculture13081530.

Zhang Z, Bian J, Han W, Fu Q, Chen S, Cui T (2018) Diagnosis of cotton water stress using unmanned aerial vehicle thermal infrared remote sensing after removing soil background. Trans. Chin. Soc. Agric. Mach. 49(10): 250-260. https://doi.org/10.6041/j.issn.1000-1298.2018.10.028.

Zhao W, Ma F, Ma H, Zhou C (2022) Soil salinity inversion model based on the multispectral images of UAV. Transactions of the CSAE. 38(24): 93-101. https://doi.org/10.11975/j.issn.1002-6819.2022.24.010.

Zhang L, Zhang H, Niu Y, Han W (2019) Mapping maize water stress based on UAV multispectral remote sensing. Remote Sens. 11(6), 605. https://doi.org/10.3390/rs11060605.

Zhang Z, Tai X, Yang N, Zhang J, Huang X, Chen Q (2022) UAV multispectral remote sensing soil salinity inversion based on different vegetation coverage. Trans. Chin. Soc. Agric. Mach. 53(8): 220-230. https://doi.org/710.6041/j.issn.1000-1298.2022.08.023.

Zhang Z, Yu G, Wu T, Zhang Y, Bai X, Yang S, Zhou Y (2021) Temperature extraction of maize canopy and crop water stress monitoring based on UAV remote sensing images. Transactions of the CSAE. 37(23): 82-89. https://doi.org/10.11975/j.issn.1002-6819.2021.23.010.